

and inverted, compared to the radiating-basis triangular element, is introduced on this antenna (Fig. 5). The goal here is to combine the matching frequencies of the two created antennas (one with $h_1 = 7.5$ mm, and the other $h_2 = 15$ mm) and thus to widen the resultant bandwidth of the structure.

This results in a VSWR of about 1.5 (Fig. 6) and a much better adaptation from 3 to 7 GHz (Fig. 7). By comparing these results with those obtained experimentally, a widening of the bandwidth after 7 GHz (which was not observed in the simulation, can be noted. This variation is certainly due to the phenomenon of loss adaptation related to the poor performances of epoxy at high frequencies. The fact that this antenna is fed by a broader CPW line than that of the preceding one (the wave only propagates in the substrate under the feeding line) may explain why this phenomenon was not perceived in the first antenna.

The addition of the slot does not disturb the radiation pattern, in comparison with the first structure, while the efficiency is better and fluctuates around 80% over the entire bandwidth (Fig. 8).

6. CONCLUSION

Two new omnidirectional antennas for short-range UWB communications have been presented; the first one amply covers the WPAN standard, and the other one presents a very good adaptation and good radiation efficiency on a very broad frequency band. Both antennas are approximately the same size as a standard business card, have low manufacturing cost, and are matched to 50Ω . Optimizations of radiation pattern and tests on better quality substrate should increase the high-frequency performances of these two antennas.

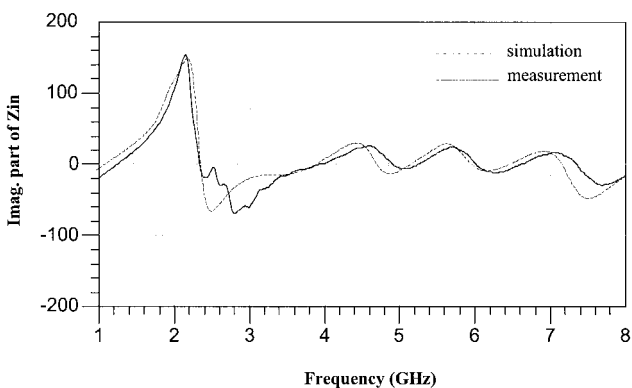
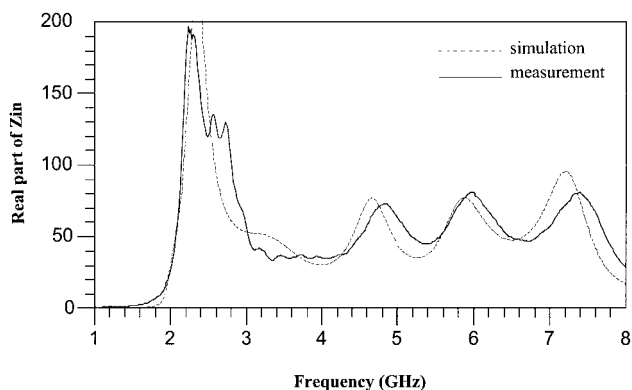


Figure 7 Real and imaginary parts of the input impedance

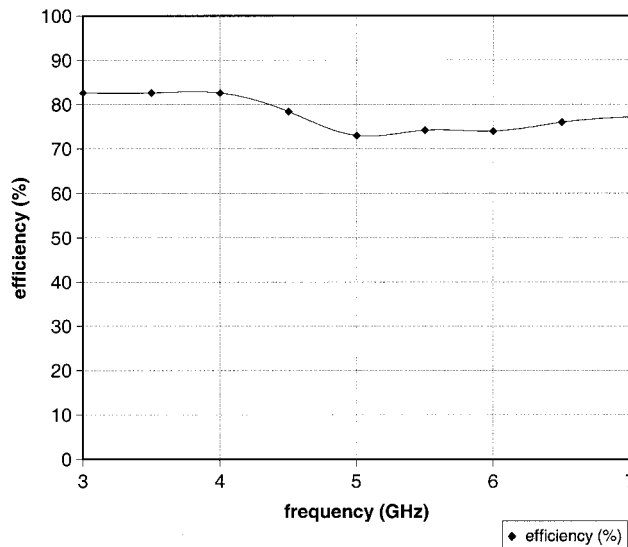


Figure 8 Radiation efficiency

REFERENCES

1. D.J. Daniels, Surface-penetrating radar, IEE Radar Sonar Navigation Avionics Series 6 (1996), 72–93.
2. J.R. Foerster, The effect of multipath interference on the performance of UWB systems in an indoor wireless channel, IEEE Semiannual Vehic Technol Conf, Rhodos, Greece 2001.
3. S.L. March, C.M. Panasik, UWB: Next generation WPAN, Int Microwave Symp UWB Wkshp, Amsterdam, Netherlands 2003.
4. R.C. Johnson, Antenna engineering handbook, 3rd ed. 1993, pp. 42–8–42–13.
5. G.H. Brown, and O.M. Woodward, Experimentally determined radiation characteristics of conical and triangular antennas, RCA Rev 13 (1952), 425–452.
6. Z.N. Chen, Experiments on input impedance of tilted planar monopole antenna, MOTL 26 (2000), 202–204.

© 2004 Wiley Periodicals, Inc.

PILOT: A FAST ALGORITHM FOR ENHANCED 3D PARASITIC CAPACITANCE EXTRACTION EFFICIENCY

Dipanjan Gope and Vikram Jandhyala

Dept. of Electrical Engineering
University of Washington
Seattle, WA 98195

Received 13 October 2003

ABSTRACT: Integral-equation methodologies applied to extract parasitics for board, package, and on-chip structures involve solving a dense system of equations. In this paper, we present an improved matrix-compression technique for fast iterative solution of such dense systems, which applies QR decomposition on multilevel oct-tree-based interaction sub-matrices. The regular-tree structure of the fast-multipole method and the rank-revealing QR-based matrix-compression scheme are combined in order to achieve superior time and memory efficiency. As is demonstrated by the numerical-simulation results presented herein, the new algorithm is found to be faster and more memory efficient than both existing QR-based methods and FastCap. © 2004 Wiley Periodicals,

Key words: method of moments; fast multipole method; low-rank compression; capacitance; integral equation

1. INTRODUCTION

Due to the increasing complexity of design structures on boards, packages, and chips, numerical techniques that utilize field solutions for parasitic extraction are preferred when high accuracy is necessary. Among the existing numerical tools, a surface-based integral-equation methodology such as the method of moments (MoM) [1] is ideally suited to address the problem. It leads to a well-conditioned system with reduced size, as compared to volumetric methods [2], but the system of equations generated is inherently dense, thereby creating a time and memory bottleneck. Several fast iterative techniques have been developed to efficiently solve a MoM system with linear time and memory complexity. All these methods, including QR-based approaches [3, 4], fast-multipole methods (FMMs) [5], and FFT-based techniques [6] accelerate matrix-vector products and therefore expedite the Krylov-subspace iterative solution [7].

The QR-based fast iterative solver (IES³) [3, 4] adopts a binary-tree multilevel decomposition of the geometry and consequent low-rank compression of the MoM sub-matrices which represent the interaction between well-separated geometrical regions. This scheme is particularly attractive for circuit problems, since it can be directly applied with multilayered dielectric Green's functions. Even in terms of free-space capacitance extraction, IES³ has been demonstrated as being more efficient in terms of memory and solve time. However, this method suffers from a higher setup-time cost, due to the irregular nature of the adopted binary-tree structure for the geometry subdivisions and the unpredictable nature of the optimal matrix structure.

In this work, we have developed a predetermined interaction list oct-tree (PILOT) QR algorithm that greatly reduces the setup time while maintaining the memory and solve-time efficiency of the rank-map-based binary tree QR (RMBT-QR), which is based on the same principles as IES³. PILOT exploits the properties of a multilevel oct-tree implementation (common to multilevel fast multipole method (FMM) approaches), to create a predetermined tree structure, thereby considerably reducing the setup time.

2. INTEGRAL EQUATION

Capacitance problems formulated using the MoM are solved via Poisson's equation $\nabla^2\phi(\mathbf{r}) = -\rho(\mathbf{r})/\epsilon$, relating potential ϕ and charge-density ρ . The discretization of the integral form of this equation results in a matrix system of the form $\bar{\mathbf{Z}}\mathbf{I} = \mathbf{V}$ where the $N \times N$ MoM matrix $\bar{\mathbf{Z}}$ is a dense Green's function matrix, \mathbf{I} represents the unknown coefficients of known charge density basis functions, and \mathbf{V} is the known potential excitation. Each element of the MoM matrix denotes the interaction between a testing and a basis function and is written as follows:

$$\bar{Z}(j, i) = \int_{S_j} ds_t(\mathbf{r}) \int_{S_i} ds' g(\mathbf{r}, \mathbf{r}') f_i(\mathbf{r}'), \quad (1)$$

where t and f are the testing and basis functions, S is their domain, and $g(\mathbf{r}, \mathbf{r}')$ is the relevant Green's function.

3. EXISTING MULTILEVEL QR ALGORITHM

The IES³ fast iterative solver reduces the cost of performing the matrix vector product $\bar{\mathbf{Z}}\mathbf{I}$ to $O(N \log N)$ from quadratic time. It is

based on using the modified Gram–Schmidt (MGS) method [8] for QR decomposition of a low-ranked interaction sub-matrix $\bar{\mathbf{A}}$ of the MoM matrix $\bar{\mathbf{Z}}$:

$$\bar{\mathbf{A}}_{m \times n} = \bar{\mathbf{Q}}_{m \times r} \bar{\mathbf{R}}_{r \times n}, \quad (2)$$

where $\bar{\mathbf{R}}$ is upper triangle, $\bar{\mathbf{Q}}$ is unitary, that is, $\bar{\mathbf{Q}}^T \bar{\mathbf{Q}} = \bar{\mathbf{I}}$ and $r \ll (m, n)$. At the same time, it is possible to construct the compressed representations without forming the entire submatrix from sampled rows and columns, thereby reducing the setup time to $O(N \log N)$.

In RMBT-QR, which is based on the same principle as IES³, the algorithm has the following three main steps.

1. Geometry subdivisions into cells. binary decompositions with density balancing and tight bounds, technically known as tightly bound k - d trees [9], are employed in a manner similar to those used in IES³.
2. Rank-map predicted QR formations. a rank-map is a statically-determined lookup table that identifies large and low-ranked submatrices for QR formation so as to ensure maximum compression with minimum setup time. Each entry of the table outlines the expected rank of a cell-to-cell interaction, which is a function of various parameters pertaining to the source and observer cells and the kernel involved.
3. Fine-tuning through splits and merges. the rank-map only predicts the starting tree structure for a MoM matrix, and the rank estimation is often inaccurate and may result in underestimation of rank or missing larger low-rank blocks. These problems are addressed by splits and merges, respectively [3].

The setup cost of the algorithm is largely controlled by the accuracy of the rank-map predictions. An accurate and exhaustive rank map would preclude the necessity for merges and unnecessary splits, and the optimum tree structure would be achieved without any backtracking or fine-tuning. However, a foolproof rank-map cannot be unfeasibly constructed, due to the fact that the algorithm can lead to cells of any shape and size. This leads to a high constant being associated with the setup-time cost of the algorithm.

4. NEW MULTILEVEL QR ALGORITHM

The proposed PILOT-QR algorithm develops a predetermined multilevel matrix structure for the geometry under consideration, which guarantees maximum compression. The algorithm has three main steps as follows.

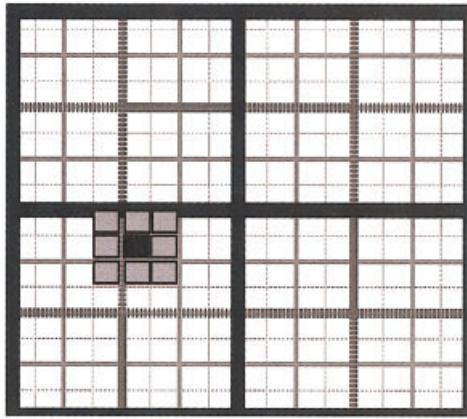
1. Oct-tree spatial decomposition in 3D. each cube is recursively decomposed by loosely bounded, spatially balanced splits along orthants [9], which leads to a maximum of eight child cubes in 3D. The cell data structure is in the form of an oct-tree, identical to that in multilevel FMMs [6].
2. Basic multilevel interaction list. every cube c_i has a nearest neighbor list [Fig. 1(a)] and an interaction list [Fig. 1(b)]. The nearest neighbor list is defined as

$$K_{c_i} = \{c_j | c_j \text{ is in the same level as } c_i$$

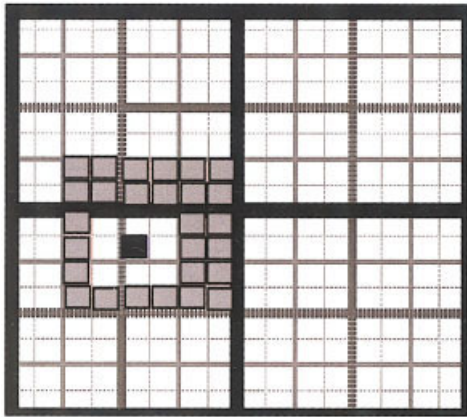
and has at least one common vertex with $c_i\}$ (3)

and the interaction list is denoted by

$$I_{c_i} = \{c_j | P_{c_j} \in K_{P_{c_i}}; c_j \notin K_{c_i}\}, \quad (4)$$



(a)



(b)

Figure 1 (a) Neighbor list and (b) interaction list for the given cube in FMM at level 4. [Color figure can be viewed in the online issue, which is available at www.interscience.wiley.com]

where P_{c_i} denotes parent of c_i . In FMM, multipole expansions are used to construct $T(c_j, c_i) \forall j|c_j \in I_{c_i}$, where $T(c_j, c_i)$ denotes the interaction between testing functions of c_j and basis functions of c_i . Since PILOT does not explicitly require cubical regions, but simply deals with interaction matrices, there is scope for further compression by combining cubes in I_{c_i} in an a priori manner into a new interaction list called the merged interaction list (MIL).

- Merged interaction list. It is observed that the interaction lists of siblings share many cubes in common, as illustrated in Figure 2 (a 2D version is shown here for ease of illustration). It is possible to group source and observer cubes of different interaction lists in order to compress larger low-rank matrices, and thereby gain, in terms of overall compressibility. The common interaction list is carefully decomposed into disjointed parts such that the overall compression is optimized. Each such disjointed part is an interaction between grouped source cubes and observer cubes and forms an entry of the MIL denoted by μ , which can be expressed as a combination of cube-to-cube interactions as follows:

$$\mu_k = \{T_p(c_j, c_i)\} \quad \forall p|1 \leq p \leq n_g, \quad (5)$$

where n_g is the number of regular interactions grouped.

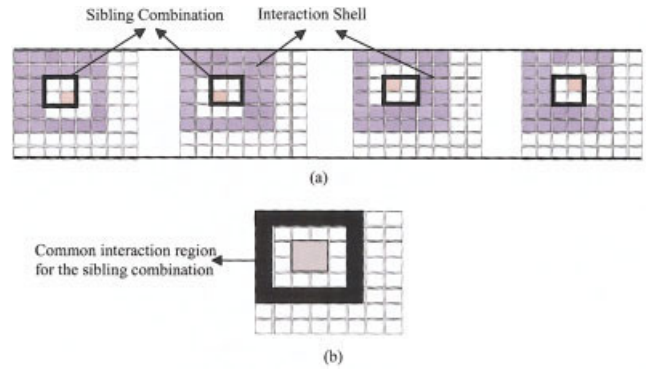


Figure 2 (a) Individual interaction shells of each cube belonging to the sibling combination; (b) common interaction shell for the sibling combination formed by the intersection of individual interaction regions of cubes belonging to the sibling combination (for visualization purposes, 2D shells are illustrated). Similar common interaction regions exist for 3D geometries. [Color figure can be viewed in the online issue, which is available at www.interscience.wiley.com.]

Higher compression is achieved, since a larger matrix is compressed to low rank, given by

$$(m_{\mu_k} + n_{\mu_k})r_{\mu_k} < \sum_{i=1}^{n_g} (m_i + n_i)r_i, \quad (6)$$

where m , n , and r denote the number of rows, number of columns, and the rank of a submatrix, respectively. The subscript i denotes a regular multilevel interaction list entry that is now a constituent of the MIL. Figure 3 demonstrates the decomposition of the common interaction list of Figure 2 into merged interactions.

In PILOT there are a total of 16 MIL entries in 2D and 40 in 3D. The same MIL pattern is valid for all sibling pairs across the levels. The MIL thus leads to a predetermined tree structure. MoM submatrices pertaining to interactions of the MIL are compressed by forming QRs from samples. At the finest level, dense blocks are retained for interactions of the smallest cube with its neighbors.

5. SIMULATION RESULTS

In this section, simulation results are presented to demonstrate the accuracy and time and memory efficiency of PILOT. For a comparative analysis, results obtained from RMBT-QR and FastCap [5] are presented side-by-side. A QR decomposition tolerance of $1e-3$ is used for both PILOT and RMBT-QR, whereas for FastCap the adaptive algorithm with a multipole order of 2 is employed. An

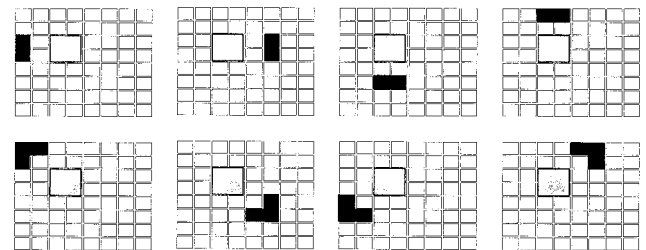


Figure 3 Merged interaction list entries corresponding to the common interaction region of Fig. 2(b). Each entry gives rise to a low-rank matrix block

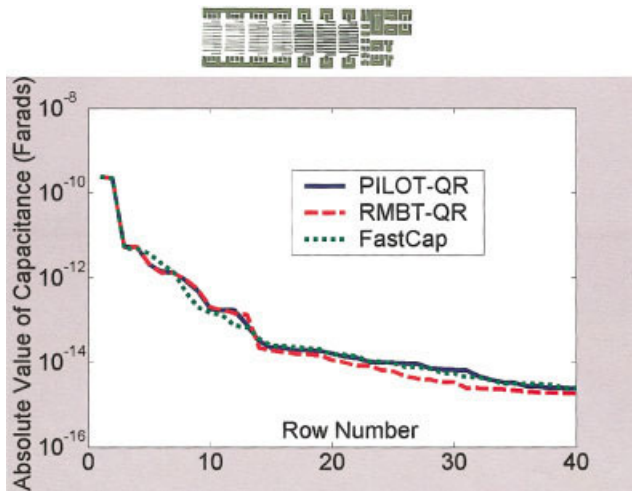


Figure 4 Absolute values of the first column of the capacitance matrix for the structure shown are plotted for all three algorithms (relative error in the capacitance matrix for all algorithms is on the order of $1e-3$). [Color figure can be viewed in the online issue, which is available at www.interscience.wiley.com.]

absolute residual of $1e-3$ is used for the Krylov subspace iterative solution. All tests were run on a processor with 4-GB RAM and 1.6-GHz CPU speed. The tolerances are chosen such that the results are of comparable accuracies for all the algorithms.

In the first example, the capacitance matrix of the multinet structure [Fig. 2(a)] is simulated for validation. The surface of the

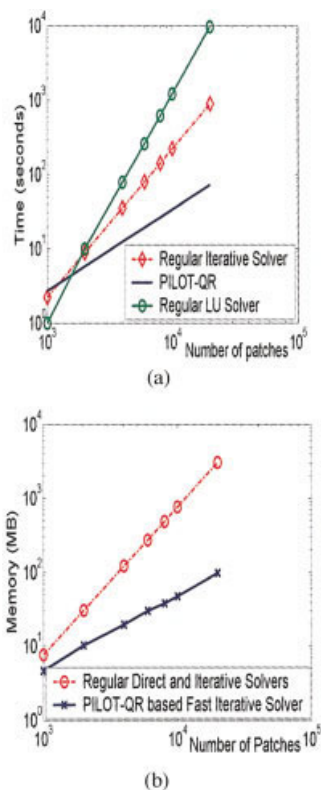


Figure 5 (a) Time and (b) memory of PILOT compared to those of the regular iterative and direct solvers. It can be observed from these logarithmic plots that PILOT requires linear time and memory, unlike the regular methods. [Color figure can be viewed in the online issue, which is available at www.interscience.wiley.com.]

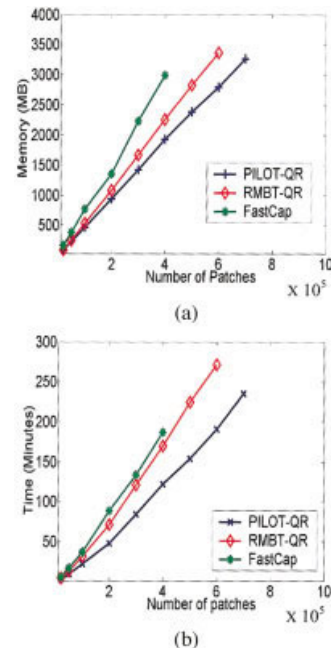


Figure 6 (a) Time and (b) memory of PILOT compared to those of the other fast solvers. It can be observed from these linear plots that PILOT has lower constants associated with its linear time and memory growths. [Color figure can be viewed in the online issue, which is available at www.interscience.wiley.com.]

structure is meshed with 0.113 million patches. The absolute values of the first column of the matrix are plotted in Figure 4.

In the next example, a 5×5 bus structure is considered. The number of triangular patches is varied from 1000 to 0.7 million. The memory efficiency of PILOT is demonstrated first by a comparison with regular direct and iterative solvers, as shown in Figure 5, and then to RMBT-QR and FastCap, as shown in Figure 6. The relative errors (Euclidean norms) in the capacitance matrices obtained by all the algorithms are on the order of $1e-3$.

The next example demonstrates the relative advantage of QR methods for a higher number of nets. A package structure with 14 leads is considered. The surface is meshed with 0.101-million patches and then solved for an increasing number of right-hand sides (1 to 14). The time requirements are plotted in Figure 7. The constant offset between the plots of PILOT and RMBT-QR is due to the superior one-time setup cost. The memory required for the process by PILOT is 441 MB, by RMBT-QR is 445 MB, and by FastCap is 700 MB.

The largest problem solved by using our method thus far is a 10×3 array of the structure in example 1. The entire geometry is discretized with 0.913-million patches. The problem took 3.3 Gb and 48 min to set up and 90 min to solve for three specific excited nets. Both the other methods could not fit the problem in the 4-Gb available.

6. CONCLUSIONS

A new oct-tree-based QR technique for fast-parasitic extraction, PILOT, has been presented. The best features of FMM and IES³ are exploited; along with the generation of new merged-interaction lists in order to yield superior run times and reduced memory consumption. In the battle of reducing constants in the era of mature linear-complexity algorithms, PILOT can potentially emerge as an optimal paradigm for parasitic extraction. While this paper is related to parasitic extraction, the PILOT paradigm can

ANALYSIS OF PHOTONIC BAND-GAP (PBG) STRUCTURES USING THE FDTD METHOD

Ming-Sze Tong,¹ Min Cheng,¹ Yilong Lu,¹ Yinchao Chen,² Viktor Krozer,³ and Rüdiger Vahldieck⁴

¹ School of Electrical and Electronic Engineering
Nanyang Technological University
Nanyang Avenue
Singapore 639798

² Department of Electrical Engineering
University of South Carolina
Swearingen Engineering Center
Columbia, SC 29208

³ EMI/Ørsted
Technical University Denmark
Ørstedplads, Build, 328
DK-2800 Kgs. Lyngby, Denmark

⁴ Institute of Field Theory and High Frequency Engineering
Swiss Federal Institute of Technology
CH-8092 Zurich, Switzerland

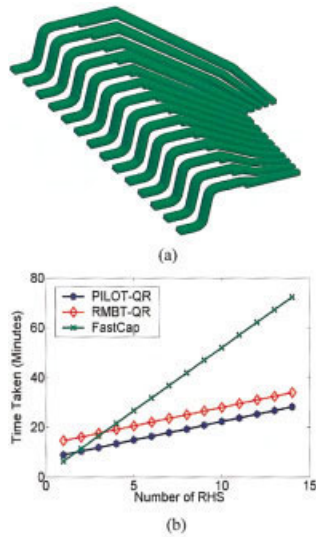


Figure 7 Performance comparison showing the efficiency of QR-based algorithms for increasing number of RHS: (a) multipin structure considered for simulation consisting of 14 pins; (b) setup and solve times for an increasing number of RHS. [Color figure can be viewed in the online issue, which is available at www.interscience.wiley.com.]

also be applied to full-save applications for small electrical structures in multilayered micro-electronic environments.

REFERENCES

1. R.F. Harrington, *Field computation by moment methods*, IEEE Press, New York, 1991.
2. T.-Y. Chou and Z.J. Cendes, Capacitance calculation of IC packages using the finite element method and planes of symmetry, *IEEE Trans CAD Integrated Circ Syst* 13 (1994), 1159–1166.
3. S. Kapur and D.E. Long, IES³: Efficient electrostatic and electromagnetic solution, *IEEE Computer Sci Engg* 5 (1998), 60–67.
4. S. Kapur and D. Long, IES³: A fast integral equation solver for efficient 3-dimensional extraction, *IEEE/ACM Int Conf CAD*, 1997, pp 448–455.
5. K. Nabors and J. White, FastCap: A multipole accelerated 3-D capacitance extraction program, *IEEE Trans CAD Integrated Circ Syst* 10 (1991), 1447–1459.
6. J.R. Phillips and J. White, A precorrected-FFT method for electrostatic analysis of complicated 3-D structures, *IEEE Trans CAD Integrated Circ Syst* 16 (1997), 1059–1072.
7. H.A. van der Vorst, Krylov subspace iteration, *Computing Sci & Engg* 2 (2000), 32–37.
8. G.H. Golub and C.F. Van Loan, *Matrix computations*, 2nd ed., Johns Hopkins University Press, Baltimore, MD, 1989.
9. R.J. Anderson, Tree data-structures for N-body simulation, *SIAM J Computing* 28 (1998), 1923–1940.

© 2004 Wiley Periodicals, Inc.

Received 6 October 2003

ABSTRACT: In this paper, a number of photonic band-gap (PBG) structures, which are formed by periodic circuit elements printed on transmission-line circuits, are studied by using a well-known numerical method, the finite-difference time-domain (FDTD) method. The results validate the band-stop filter behavior of these structures, and the computed results generally match well with ones published in the literature. It is also found that the FDTD method is a robust, versatile, and powerful numerical technique to perform such numerical studies. The proposed PBG filter structures may be applied in microwave and communication systems. © 2004 Wiley Periodicals, Inc. *Microwave Opt Technol Lett* 41: 173–177, 2004; Published online in Wiley InterScience (www.interscience.wiley.com). DOI 10.1002/mop.20084

Key words: PBG; FDTD; microstrip

1. INTRODUCTION

Recently, there have been a number of studies on photonic band-gap (PBG) structures in the area of electromagnetism and communications systems. PBGs are structures typically formed by periodic circuit elements, in which a band-gap filter behavior is exhibited in a certain frequency range. They were first proposed in the area of optics, as given in [1], but were then applied in the microwave area [2, 3] by downscaling the operating frequencies.

In this paper, a number of PBG planar structures printed on transmission-line circuits, such as microstrip lines, coplanar waveguides, and striplines, are studied using a well-known numerical method called the finite-difference time-domain (FDTD) method [4]. These PBG circuits can be diversely applied into microwave and communications systems, such as the printed circuit boards (PCB) in computer motherboards or mobile antennas. The circuit characteristics, particularly their band-gap filtering nature, are validated through the analysis of the *S* parameters. Results also show that the FDTD method is robust, versatile, and reliable for such numerical calculations.

2. FDTD METHOD AND COMPUTATIONAL SETUP

The main idea of the FDTD lies on solving the Maxwell's curl equation pair:

$$\nabla \times \vec{H} = \frac{\partial \vec{D}}{\partial t} + \vec{J} \quad \text{and} \quad \nabla \times \vec{E} = -\frac{\partial \vec{B}}{\partial t} - \vec{M}. \quad (1)$$